

## Amorphous Mg-based metal foams with ductile hollow spheres

A. H. Brothers, D. C. Dunand, Q. Zheng, and J. Xu

Citation: *Journal of Applied Physics* **102**, 023508 (2007);

View online: <https://doi.org/10.1063/1.2756043>

View Table of Contents: <http://aip.scitation.org/toc/jap/102/2>

Published by the *American Institute of Physics*

---

### Articles you may be interested in

[Syntactic bulk metallic glass foam](#)

*Applied Physics Letters* **84**, 1108 (2004); 10.1063/1.1646467

[Amorphous metallic foam](#)

*Applied Physics Letters* **82**, 370 (2003); 10.1063/1.1537514

[Enhancement of room-temperature plasticity in a bulk metallic glass by finely dispersed porosity](#)

*Applied Physics Letters* **86**, 251907 (2005); 10.1063/1.1953884

[Mg-based metallic glass/titanium interpenetrating phase composite with high mechanical performance](#)

*Applied Physics Letters* **95**, 171910 (2009); 10.1063/1.3257699

[Bulk metallic glass matrix composites](#)

*Applied Physics Letters* **71**, 3808 (1998); 10.1063/1.120512

[Metallic glass matrix composite with precipitated ductile reinforcement](#)

*Applied Physics Letters* **81**, 1020 (2002); 10.1063/1.1498864

---

**Scilight**

Sharp, quick summaries **illuminating**  
the latest physics research

Sign up for **FREE!**



## Amorphous Mg-based metal foams with ductile hollow spheres

A. H. Brothers and D. C. Dunand<sup>a)</sup>

*Department of Materials Science and Engineering, Northwestern University, Evanston, Illinois 60208*

Q. Zheng and J. Xu

*Shenyang National Laboratory for Materials Science, Institute of Metal Research, Chinese Academy of Sciences, Shenyang, 110016, China*

(Received 2 May 2007; accepted 21 May 2007; published online 18 July 2007)

To date, high compressive ductility and energy absorption have been achieved in amorphous metal foams based on high-toughness Pd- and Zr-based metallic glasses and are known to result from two extrinsic toughening mechanisms: bending of struts and shear band arrest by pores. We study here a syntactic amorphous metallic foam produced by infiltration of a bed of hollow crystalline iron spheres with a low-toughness Mg-based metallic glass ( $\text{Mg}_{60}\text{Cu}_{21}\text{Ag}_7\text{Gd}_{12}$ ). After quenching to vitrify the matrix, this foam exhibits much higher compressive failure strain and energy absorption than the monolithic metallic glass, an improvement which is assigned to an intrinsic mechanism, i.e., composite toughening by the network of hollow ductile iron spheres. © 2007 American Institute of Physics. [DOI: 10.1063/1.2756043]

### I. INTRODUCTION

Despite several interesting and promising properties (e.g., high strength, wear resistance, and corrosion resistance), most amorphous metals suffer from poor ductility in both tension and compression. Several solutions have been developed to address this problem,<sup>1–3</sup> one of which is the processing of amorphous metal foams. As reviewed recently,<sup>4,5</sup> previous work has shown that amorphous foams can enjoy compressive ductility and energy absorption comparable to, or even better than, those of foams made from ductile crystalline metals such as aluminum.<sup>6,7</sup> The two mechanisms underlying these improvements—interruption of shear bands by pores and stabilization of shear bands within thin foam struts deformed in bending—appear to be extrinsic in nature, i.e., they are due to the architecture of the foam rather than the intrinsic toughness of the alloy. However, the work on mechanical properties to date<sup>6–10</sup> has focused on Zr- and Pd-based alloys which, among amorphous metals, have very high toughness.<sup>11</sup> For this reason, it is not certain whether such extrinsically induced improvements in compressive ductility could persist in amorphous metallic foams whose base alloys are more brittle. In fact, foams made of highly brittle crystalline or amorphous ceramics behave in a brittle manner: they crush during compressive deformation with very little energy absorption and large-scale fracturing.<sup>12</sup>

As-cast amorphous Zr-based alloys, such as those used in earlier foam research,<sup>6</sup> have fracture energies<sup>11</sup> in the range of 70–100 kJ/m<sup>2</sup>. There is interest in foaming stronger or lighter amorphous alloys (e.g., those based on iron or magnesium, respectively), but they exhibit much lower fracture energies ( $\sim 0.1$  kJ/m<sup>2</sup> for Mg alloys), often comparable to those of silicate glasses ( $\sim 0.003$  kJ/m<sup>2</sup>).<sup>11</sup> A

recent article<sup>13</sup> reported extremely low compressive fracture strengths (1–10 MPa) for an amorphous  $\text{Fe}_{48}\text{Cr}_{15}\text{Mo}_{14}\text{Y}_2\text{C}_{15}\text{B}_6$  alloy with  $\sim 58\%$ – $65\%$  porosity, despite intracellular solid regions as thin as a few micrometers, well below the value at which bending ductility of the struts providing compressive ductility in Zr-based metallic foams would be expected.<sup>14</sup> These very low compressive strength and ductility were assigned to the low fracture toughness value of this Fe-based alloy (3 MPa m<sup>1/2</sup>), which together with a yield strength of  $\sim 4$  GPa results in a submicrometer plastic zone size.<sup>13</sup> Crack nucleation from microstructural defects and embrittlement due to the hydrogen used to produce the pores were offered as explanations for the brittleness of this foam.

Mg-based bulk amorphous alloys, the first of which were discovered in the 1990s,<sup>15</sup> are of interest because of their low densities as compared to most other amorphous alloys (and in particular the Pd,<sup>7,9,10</sup> Fe,<sup>13</sup> and Zr alloys<sup>6,8,16,17</sup> used so far for foams; other amorphous metal foams<sup>18–21</sup> are not considered here, as the toughness of these alloys, or the mechanical properties of the foams, are not as well known) and because of their low melting temperatures, simplifying the foaming process.<sup>4,22</sup> In view of the recent results of brittle Fe-based amorphous foams,<sup>13</sup> foaming low-toughness Mg-based amorphous alloys seems unlikely to result in improvements in compressive strains and energy absorption through the earlier extrinsic mechanisms based on shear band stabilization.

Instead, we explore here another approach based on the addition of a ductile phase to the amorphous matrix of the foam, which has been found to improve compressive ductility and energy absorption in nonporous amorphous composites.<sup>2,3,23</sup> Rather than using ductile fibers or particulates of crystalline metals such as W, Nb, or Mo, as done previously for amorphous metals composites,<sup>24–26</sup> we add to the matrix a continuous network of hollow iron spheres

<sup>a)</sup>Author to whom correspondence should be addressed; electronic mail: dunand@northwestern.edu

which act both as ductilizers (as in composites) and as pore formers (as in other “syntactic” foams). These syntactic foams are structurally and mechanically characterized and compared with earlier amorphous metal foams. This study, in addition to being the first to report foams based on a Mg-based amorphous alloy, is also the first to use ductile phase toughening as a mechanism to improve foam mechanical properties.

## II. EXPERIMENTAL PROCEDURES

The alloy used in this work,  $\text{Mg}_{60}\text{Cu}_{21}\text{Ag}_7\text{Gd}_{12}$ , has a critical casting diameter of  $\sim 17$  mm for complete glass formation, which is smaller than the 25 mm value for the optimal composition<sup>27</sup> at  $\text{Mg}_{54}\text{Cu}_{26.5}\text{Ag}_{8.5}\text{Gd}_{11}$ , but is sufficient to ensure the formation of a monolithic amorphous phase for the specimen sizes (as-cast diameters  $\sim 8$  mm) used here. The alloy used here has a low glass transition temperature of  $157$  °C and a large supercooled-liquid region (crystallization temperature  $192$  °C), as measured by differential scanning calorimetry (DSC) at a rate of  $20$  °C/min.<sup>27</sup>

The foams were created by pressure infiltrating the molten alloy into beds of hollow spheres, a method which has been used previously for producing syntactic foam materials from various crystalline alloys<sup>28–31</sup> and one Zr-based amorphous metal.<sup>32</sup> In the present work, we used iron hollow spheres provided by the Fraunhofer Institute (Dresden, Germany). Chemical analysis of the spheres revealed the presence of  $0.21$  wt % O and  $0.043$  wt % C, together with small amounts ( $0.01$ – $0.02$  wt %) of Si, V, Cr, Mn, and Ni. Measurement of 30 individual spheres using a balance and micrometer showed a sphere diameter of  $1.87 \pm 0.10$  mm, net sphere density (sphere mass/sphere volume) of  $1.0 \pm 0.1$  g/cm<sup>3</sup>, sphere relative density of  $12.5 \pm 1.5\%$ , and corresponding sphere wall thickness (assuming spherical shape with uniform wall thickness) of  $41 \pm 5$   $\mu\text{m}$ . Packing of large numbers of spheres into stainless steel infiltration crucibles (inner diameter  $8.1$  mm) showed a mean tap-dense packing fraction of  $48\%$ , below the expected value of  $64 \pm 4\%$  due to disruption in packing efficiency caused by the small ratio of container diameter to sphere diameter.<sup>33</sup>

Tap-dense sphere beds were placed into infiltration crucibles and sintered under high vacuum conditions ( $10^{-3}$ – $5 \times 10^{-3}$  Pa) for 4 h at  $1250$  °C. Spheres were found to be diffusion bonded to one another and to the crucible wall, thus preventing sphere redistribution during infiltration. A first sintered sphere bed was removed from its crucible by electric discharge machining, forming a cylindrical compression specimen with  $6.0$  mm diameter and  $12.7$  mm height. The measured packing density of spheres in this machined specimen was  $57\%$ , slightly higher than measured by simple packing experiments. This is most likely a result of the fact that the material nearest the crucible wall, whose packing is typically least efficient, was removed during machining. The specimen density was calculated as  $0.57$  g/cm<sup>3</sup>, corresponding to a relative density (as compared to pure iron) of  $7.3\%$ . Another sintered bed was evacuated, heated to  $575$  °C, and pressure-infiltrated with molten  $\text{Mg}_{60}\text{Cu}_{21}\text{Ag}_7\text{Gd}_{12}$  using an argon pressure of  $153$  kPa, applied for about 1 min. After

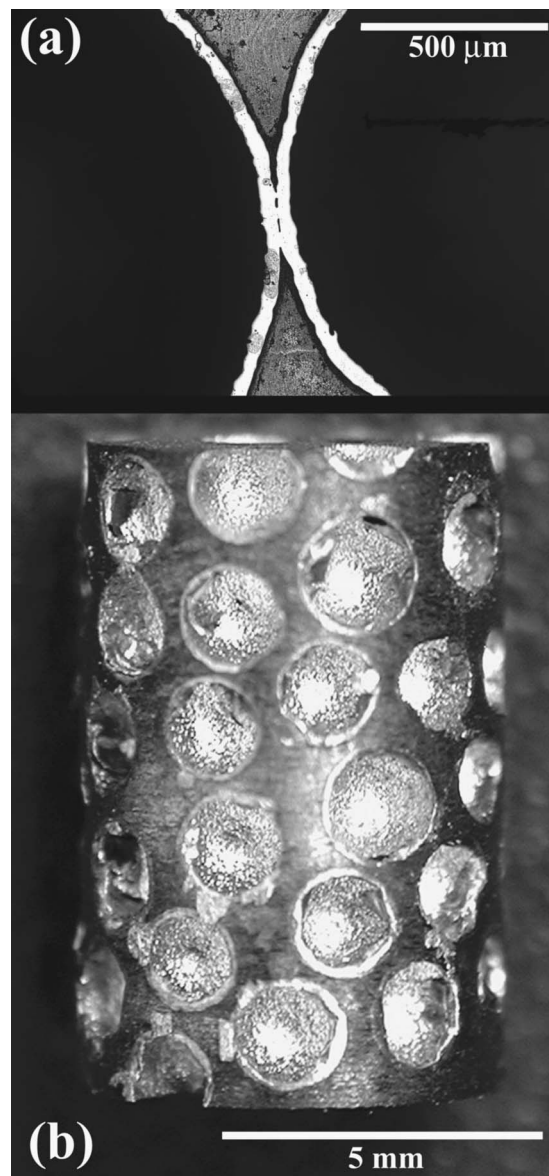


FIG. 1. Images of the as-cast (amorphous) foam structure. (a) Micrograph of a polished slice taken from the bottom of the cast foam, showing the infiltrated matrix region between two iron spheres. (b) Photograph of the macroscopic structure of the amorphous foam prior to testing. The wall thickness of the spheres appears exaggerated by burrs produced during sample grinding.

infiltration, the steel crucible containing the molten specimen was quenched in strongly agitated chilled brine to ensure vitrification of the matrix. This infiltrated specimen was machined with a diamond grinding wheel and diamond wafering saw into two uniform cylindrical compression samples. One of these (shown in Fig. 1(b), with  $6.7$  mm diameter,  $10.1$  mm height, and  $2.25 \pm 0.01$  g/cm<sup>3</sup> bulk density) was tested in the as-cast state. The other (with  $6.6$  mm diameter,  $10.1$  mm height, and  $2.31 \pm 0.01$  g/cm<sup>3</sup> bulk density) was crystallized by vacuum annealing for 3 h at  $200$  °C.

## III. RESULTS AND DISCUSSION

No residual porosity was visible in polished cross sections from identically prepared samples; rather, the alloy was found to infiltrate even small gaps between spheres (Fig.

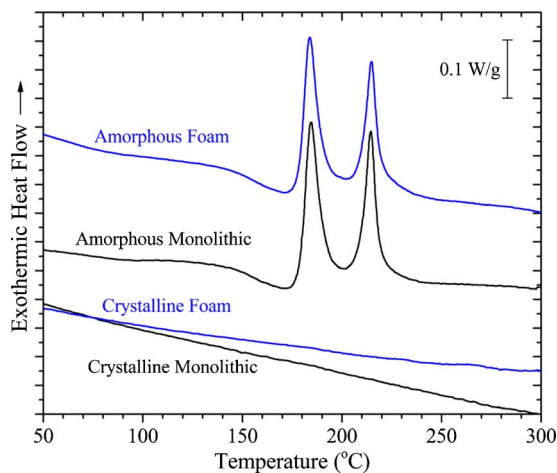


FIG. 2. DSC traces from Mg-based amorphous metal, both monolithic and foamed, at a constant heating rate of 5 °C/min. Shown for comparison are the traces of the crystalline monolithic alloy and the foam crystallized by annealing at 200 °C for 3 h.

1(a)). Metallographic preparation was made difficult by the corrosion susceptibility of the alloy, however, and thus fine porosity could have escaped detection. Metallographic specimens did reveal, however, macroscopic uniformity in foam structure and absence of infiltration into the sphere interiors. In addition, large contiguous matrix regions ( $>1$  mm in extent in cross sections) were seen within the foams. Many such matrix regions are visible in the photograph in Fig. 1(b) and they are most likely too large to allow for shear band stabilization during bending.<sup>6,14</sup> Assuming no unfiltered residual porosity between the spheres, the densities of the as-cast, amorphous and annealed, crystallized samples correspond (using the density of the solid alloy, 4.4 g/cm<sup>3</sup>, measured by helium pycnometry) to sphere volume fractions of  $63 \pm 2\%$  and  $61 \pm 2\%$ , respectively, somewhat higher than the 57% value measured for the sintered bed. Using an average sphere volume fraction of 62%, the foam relative density (as compared to the solid pure alloy) was 52% and it consisted of 57.5 vol % porosity, 38 vol % amorphous (or crystallized) Mg-based matrix, and 4.5 vol % crystalline Fe. Thus the proportion of ductile Fe phase in the solid material within the foam was 10.6 vol %.

Both monolithic and foamed Mg<sub>60</sub>Cu<sub>21</sub>Ag<sub>7</sub>Gd<sub>12</sub> were investigated by DSC at a constant heating rate of 5 °C/min. Figure 2 shows the DSC trace of the monolithic alloy, melted and cast under conditions identical to those used in foaming experiments. Also shown is the trace of the same specimen, tested in a second run to illustrate the behavior of the crystalline alloy (the alloy, as shown by the trace from the first run, had crystallized well below the maximum temperature of the first scan). Also shown in Fig. 2 is the DSC trace of a fragment of matrix from the as-cast foam, following compressive testing. This trace was nearly identical to that of the dense alloy, with an endothermic glass transition at 144 °C (compared to 145 °C for the monolithic alloy) and a two-stage crystallization event beginning at an onset temperature of 176 °C (compared to 177 °C for the monolithic alloy), indicating that foam processing did not lead to significant deterioration in the glass-forming ability of the alloy. The

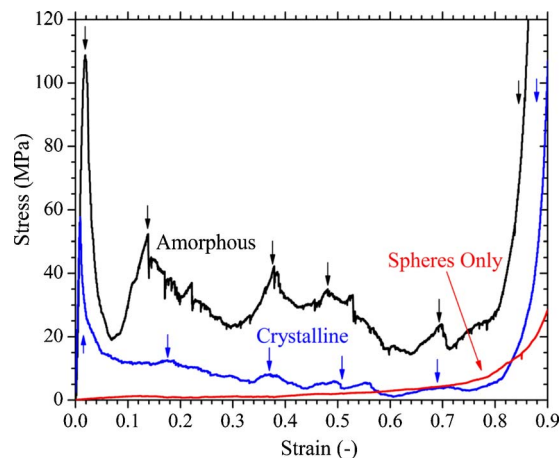


FIG. 3. Compressive stress-strain curves for the amorphous and crystalline syntactic foams and the matrix-free sintered sphere specimen. The arrows mark significant local maxima in the curve, interpreted as caused by the collective collapse of sphere layers.

transition temperatures measured here were below those measured previously<sup>27</sup> (157 and 192 °C), due to the lower heating rate used here (5 vs. 20 °C/min). Finally, Fig. 2 shows a DSC trace from a matrix fragment from the annealed specimen, which confirms that the annealing treatment is sufficient to completely devitrify the matrix. These observations were also confirmed using x-ray diffraction (not shown), where a diffuse amorphous feature was found in the absence of any measurable crystalline reflections.

The matrix-free sintered sphere specimen and the as-cast and annealed foams (hereafter referred to as amorphous and crystalline foams, respectively) were tested in uniaxial compression at a nominal strain rate of  $5 \times 10^{-4}$  s<sup>-1</sup> and their stress-strain curves are shown in Fig. 3. While it is normally desirable to have minimum specimen dimensions at least seven times greater than the pore size to improve reproducibility in foam properties,<sup>34</sup> this was not possible for these foams because of restrictions in available sphere diameter and maximum casting diameter for the alloy. Based on sphere and sample volumes, the number of spheres in each foam was about 65, which is large despite these limitations. Also tested, at a nominal strain rate of  $10^{-4}$  s<sup>-1</sup>, were five rectangular ( $4 \times 4 \times 8$  mm) samples of dense, amorphous Mg<sub>60</sub>Cu<sub>21</sub>Ag<sub>7</sub>Gd<sub>12</sub>. Their measured compressive fracture strength was  $721 \pm 25$  MPa and all specimens catastrophically failed without detectable plasticity. The Young's modulus of the alloy is estimated to be  $54 \pm 1$  GPa, based on ultrasonic measurements from bulk amorphous alloys of similar composition.<sup>35</sup>

The amorphous foam showed quasilinear loading up to a stress of 109 MPa and an engineering strain of 1.9% (Fig. 3). On the basis of density, this strength is within the trend line of previous data from amorphous metal foams, being higher than the less-dense Zr-based foams but lower than the denser Pd-based foams;<sup>5</sup> the apparent yield strain is also comparable to these amorphous and other crystalline metallic foams.<sup>12</sup> The initial loading stiffness was  $\sim 8.5$  GPa and also lies on the trend predicted by prior Pd- and Zr-based amorphous foam data.<sup>5</sup> Macroscopic yielding in the present foam was

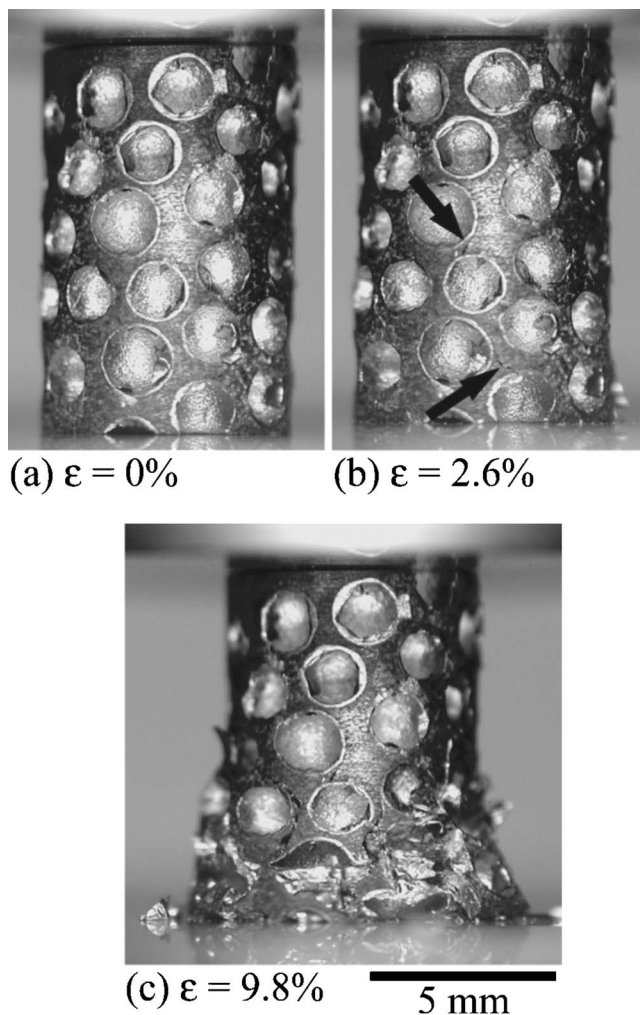


FIG. 4. Photographs showing the amorphous foam at three applied compressive strains, spanning the range of loading and initial stress drop. The arrows in panel (b) highlight matrix fractures. A crush band at the lowest section of the foam is visible in panel (c).

accompanied by a steep but smooth drop in flow stress, followed by an extended “plateau” region at about 30 MPa, consisting of periodic increases and decreases in flow stress punctuated by numerous sharp “serrations.” Release of millimeter-size fragments of matrix material was visible throughout the plateau region, and fracture was visible in the matrix at strains of around 2.5%, as shown by the arrows in Fig. 4(b) and appearing more clearly in Fig. 4(c). However, until high strains ( $\sim 60\%$ ), the foam remained mostly intact, i.e., there was no sample-wide shattering or brittle crushing as in fully brittle ceramic foams.<sup>12</sup> Final densification began at approximately 80% engineering strain; at this point, most of the matrix material had fractured and separated from the crushed foam. The energy absorbed by the foam up to a strain of 80% was  $24 \text{ MJ/m}^3$  (11 MJ/Mg). Using the average flow stress at 25% strain (29 MPa), the energy absorption of the syntactic foam falls exactly on the trend line for Zr-based amorphous metal foams<sup>6</sup> and is larger on a per-volume basis than the energy absorption of crystalline aluminum foams with the same flow stress.<sup>34</sup> On a per-weight basis, however, the Mg-based foam was inferior to these Zr-based amorphous foams<sup>6</sup> and in the lower range of aluminum foams with the same flow stress.<sup>34</sup>

By contrast, the maximum stress (i.e., strength) of the crystalline foam was markedly lower (about 57 MPa, Fig. 3), as were the loading stiffness (7 GPa) and the strain at which the initial stress drop occurred ( $\sim 0.9\%$ ). The effects of increasing strain were qualitatively similar to those in the amorphous foam, with fragments of matrix material being expelled throughout the plateau region, but the size of these fragments was generally smaller. Once again, cracks were visible from the surface at strains  $< 3\%$ , and strain was visibly nonuniform within the sample, showing evidence of strain localization as in the amorphous foam (Fig. 4(c)). In addition, the crystalline foam showed obvious macroscopic cracking (i.e., shedding of large sections of matrix) beginning around 40% strain, where no such major failure was evident in the amorphous foam. Even continuing past this event to a strain of 80%, the energy absorption of the crystalline foam was much reduced at  $6.2 \text{ MJ/m}^3$  (2.7 MJ/Mg), as compared to the amorphous foam. This makes it markedly inferior to both Zr-based amorphous metal foams<sup>6</sup> and to crystalline aluminum-alloy foams.<sup>34</sup>

The compressive behavior of the sintered sphere specimen was different than either foam, and more characteristic of a ductile foam material, with no stress drop at the macroscopic yield point, and a smoothly increasing and prolonged plateau region.<sup>12</sup> The strength of this sintered-sphere specimen was about 1 MPa, substantially below either of the foam specimens (as expected on account of its much lower density) and the specimen showed no sign of fragmentation or macroscopic failure even at high strains.

The most prominent feature in the compressive behavior of the foams is the sharp loss in flow stress following yield. Although this behavior is often observed in brittle foams,<sup>12</sup> similar (although less pronounced) stress drops have been observed previously in syntactic crystalline aluminum foams containing hollow alumina<sup>36</sup> and silica/mullite<sup>29</sup> spheres and in syntactic epoxy foam containing hollow glass spheres.<sup>37</sup> The consensus among these studies is that stress drops at yield reflect the formation of crush bands (i.e., collective fracture of individual planes of spheres) along planes of maximum stress; the loss of load-bearing capacity in the foam is therefore caused by loss of the strengthening provided by the ceramic spheres. In the present work, however, it is expected that the iron spheres (being thin walled as well as annealed during the sintering step) contribute much less to the overall load-bearing capacity than the matrix. Such a view is supported by the low strength of the sintered sphere specimen in Fig. 3. It is also noted that there are no stress drops found either in the sintered sphere specimen or in an aluminum-alloy-matrix foam containing nearly identical spheres (59 vol % unsintered iron spheres of diameter  $3.7 \pm 0.2 \text{ mm}$ , wall thickness  $\sim 200 \text{ }\mu\text{m}$ ),<sup>30</sup> where matrix and sphere contributions to strength were likely more balanced.

The stress drop at yield in the present amorphous foam is, on this basis, believed to result from loss of load-bearing capacity in the strong amorphous matrix, rather than in the weaker sphere reinforcement. Examination of Fig. 4 clearly shows that, for an average specimen strain of 9.8% (corresponding to the first stress minimum in the stress-strain

curve), deformation was highly localized in a crush band at the lowest section of the foam, with local strain (estimated from the images) reaching values as high as  $\sim 40\%$ . Matrix crushing (accompanied by sphere plastic deformation) is the most likely deformation mechanism, rather than stable shear band propagation, which in amorphous metals does not normally lead to loss in flow stress.<sup>14,38,39</sup> This is also consistent with the formation of cracks in the matrix at low strains ( $<1\%$  after yield). Thus the situation in the present foam is not dissimilar in nature to that of the brittle-sphere foams listed earlier, except for the fact that, in the present case, fracture at yield takes place in the majority phase (the matrix), rather than in the minority phase (the sphere reinforcement). The larger volume fraction of the matrix as compared to the sphere walls, along with its higher strength, explains the relatively large stress drop in the present foams. The well-known deterioration of strength and elastic strain accompanying devitrification of amorphous metals further explains the lower strength and stress drop in the crystalline foam.

Nonetheless, neglecting the contribution of the spheres, the predicted strength  $\sigma$  of the amorphous foam (using the alloy strength  $\sigma_s$  given earlier and a matrix fraction  $f$  of  $37 \pm 2\%$ ) according to the standard Gibson–Ashby relation<sup>12,34</sup>

$$\sigma/\sigma_s \sim (0.3 \pm 0.15)f^{1.5}, \quad (1)$$

lies in the range of 22–79 MPa (49 MPa, using average values), well below the measured peak value of 109 MPa, but comparable to the plateau stress of 15–50 MPa (Fig. 3). Thus, so long as the matrix remains intact and is thereby able to restrict or prevent the collapse of the spheres, the spheres can contribute noticeably to the overall load-bearing capacity. At a critical stress, matrix fracture occurs and load is transferred to the nearby spheres, which are no longer confined and then deform. Further deformation occurs by collapse of those spheres, with a gradually diminishing resistance offered by the fracturing nearby matrix.

According to this explanation, the large-scale fluctuations in load-bearing capacity visible in the plateau region of the amorphous foam reflect successive large matrix fracture events, accompanied by collapse of the surrounding iron spheres. As the number of these fluctuations (about six in Fig. 3, highlighted by arrows) corresponds to the number of spheres along the gauge length of the specimen, it is believed that each fluctuation reflects vertical propagation of the crush band by about one pore diameter, i.e., through one horizontal plane of spheres. The larger number of smaller fluctuations, or serrations, is interpreted as individual fracture events<sup>8</sup> in which a crack forms and is then halted by intersection with a sphere.

It is noted that six local maxima are found in the stress-strain curve of the crystalline foam as well (arrows in Fig. 3), probably again corresponding to collapse of sphere planes. The smaller amplitude of these fluctuations reveals a less energetic fracture, as expected given the lower strength and toughness of the crystalline matrix. The fact that expelled matrix fragments were smaller and more numerous in the crystalline foam also suggests a more distributed fracture

process. An abundance of fracture paths in the crystalline matrix is plausible, since it contained large number of brittle intermetallic inclusions and grain boundaries, unlike the homogeneous amorphous matrix of the amorphous foam, where fracture paths were likely confined to planes of maximum stress within large, uniform matrix regions, or interfaces with the spheres. It is further believed that the release of these smaller matrix fragments led to proportionally smaller changes in load-bearing area at each fracture, and thus to less pronounced serrations. Indeed, numerous small serrations are visible in the data, although they are not visible at the scale of Fig. 3.

In both foams, then, matrix cracks were intercepted, deflected, and/or blunted by the highly ductile iron sphere walls, and thus did not lead to immediate specimen failure. This resulted from the fully interconnected structure of the sintered ductile iron sphere network, which prevented propagation of continuous cracks across the whole specimen cross section by intercepting those cracks and dissipating their energy via plasticity. These toughening mechanisms, however, are active in both the amorphous and crystalline foams, and are similar to those active in interpenetrating ductile-phase-toughened ceramics such as cemented carbides;<sup>40</sup> for this reason, they do not imply matrix plasticity per se, despite the very high compressive strains achieved.

#### IV. CONCLUSIONS

This work describes the first amorphous metallic foams incorporating a network of crystalline metallic hollow spheres which acts both as a pore former and as a toughening phase, as well as the first foam made from a low-density, low-melting Mg-based amorphous metal. It is shown here that incorporation of a network of ductile iron spheres very considerably improved the compressive failure strain and energy absorption of the amorphous  $\text{Mg}_{60}\text{Cu}_{21}\text{Ag}_7\text{Gd}_{12}$  alloy. Comparison against recently studied Fe-based amorphous metal foams without ductile reinforcement<sup>13</sup> implies that the presence of the ductile iron phase, representing a modest 10.6 vol % of the solid phase in the foam, was central to achieving these improvements.

Nonetheless, fracture of the amorphous phase was still the dominant mode of deformation in the present foam, unlike several earlier foams based on tougher Zr and Pd alloys, where plasticity by shear banding prevailed. Thus, the present work demonstrates that foam architectures, even combined with ductile phases, cannot guarantee plasticity in amorphous metals. Prior improvements in amorphous foam compressive ductility by reduction in pore size<sup>6</sup> indicate that a similar approach may be useful in the current system as well. Addition of a discontinuous ductile phase in the matrix by precipitation or infiltration, as done for monolithic amorphous metals,<sup>2,3,23,24,26</sup> is another possible approach.

#### ACKNOWLEDGMENTS

The authors thank the Fraunhofer Institute for providing the iron spheres used in this work and M. Cox of Northwest-

ern University for sintering and testing the matrix-free specimen. Q.Z. and J.X. are supported by the National Natural Science Foundation of China.

- <sup>1</sup>J. Schroers and W. L. Johnson, Phys. Rev. Lett. **93**, 255506 (2004).
- <sup>2</sup>U. Kuhn, J. Eckert, N. Mattern, and L. Schultz, Appl. Phys. Lett. **80**, 2478 (2002).
- <sup>3</sup>H. Choi-Yim, R. D. Conner, F. Szuecs, and W. L. Johnson, Acta Mater. **50**, 2737 (2002).
- <sup>4</sup>A. H. Brothers and D. C. Dunand, Scr. Mater. **54**, 513 (2006).
- <sup>5</sup>A. H. Brothers and D. C. Dunand, to appear in MRS Bulletin (2007).
- <sup>6</sup>A. H. Brothers and D. C. Dunand, Acta Mater. **53**, 4427 (2005).
- <sup>7</sup>T. Wada, M. Kinaka, and A. Inoue, J. Mater. Res. **21**, 1041 (2006).
- <sup>8</sup>A. H. Brothers, D. W. Prine, and D. C. Dunand, Intermetallics **14**, 857 (2006).
- <sup>9</sup>T. Wada and A. Inoue, Mater. Trans. **44**, 2228 (2003).
- <sup>10</sup>T. Wada, A. Inoue, and A. L. Greer, Appl. Phys. Lett. **86**, 251907 (2005).
- <sup>11</sup>J. J. Lewandowski, M. Shazly, and A. S. Nouri, Scr. Mater. **54**, 337 (2006).
- <sup>12</sup>L. J. Gibson and M. F. Ashby, *Cellular Solids: Structure and Properties*, 2nd ed. (Cambridge University Press, Cambridge, 1997).
- <sup>13</sup>M. D. Demetriou, G. Duan, C. Veazey, K. De Blauwe, and W. L. Johnson, Scr. Mater. **57**, 9 (2007).
- <sup>14</sup>R. D. Conner, W. L. Johnson, N. E. Paton, and W. D. Nix, J. Appl. Phys. **94**, 904 (2003).
- <sup>15</sup>A. Inoue and T. Masumoto, Mater. Sci. Eng., A **133**, 6 (1991).
- <sup>16</sup>K. Q. Qiu and Y. L. Ren, J. Mater. Sci. Technol. **21**, 788 (2005).
- <sup>17</sup>G. Xie, W. Zhang, D. V. Louzguine-Luzgin, H. Kimura, and A. Inoue, Scr. Mater. **55**, 687 (2006).
- <sup>18</sup>J. Jayaraj, B. J. Park, D. H. Kim, W. T. Kimc, and E. Fleury, Scr. Mater. **55**, 1063 (2006).
- <sup>19</sup>M. H. Lee and D. J. Sordelet, Appl. Phys. Lett. **89**, 021921 (2006).
- <sup>20</sup>M. H. Lee and D. J. Sordelet, Scr. Mater. **55**, 947 (2006).
- <sup>21</sup>A. Gebert, A. A. Kundig, L. Schultz, and K. Hono, Scr. Mater. **51**, 961 (2004).
- <sup>22</sup>A. H. Brothers, R. Scheunemann, J. D. DeFouw, and D. C. Dunand, Scr. Mater. **52**, 335 (2005).
- <sup>23</sup>J. C. Lee, Y. C. Kim, J. P. Ahn, and H. S. Kim, Acta Mater. **53**, 129 (2005).
- <sup>24</sup>R. D. Conner, H. Choi-Yim, and W. L. Johnson, J. Mater. Res. **14**, 3292 (1999).
- <sup>25</sup>H. Choi-Yim, J. Schroers, and W. L. Johnson, Appl. Phys. Lett. **80**, 1906 (2002).
- <sup>26</sup>J. Das, W. Loser, U. Kuhn, J. Eckert, S. K. Roy, and L. Schultz, Appl. Phys. Lett. **82**, 4690 (2003).
- <sup>27</sup>H. Ma, L. L. Shi, J. Xu, Y. Li, and E. Ma, Appl. Phys. Lett. **87**, 181915 (2005).
- <sup>28</sup>Z. Y. Dou, G. H. Wu, L. T. Jiang, B. S. Ding, and J. H. Cao, Trans. Nonferrous Met. Soc. China **16**, S1634 (2006).
- <sup>29</sup>D. K. Balch, J. G. O'Dwyer, G. R. Davis, C. M. Cady, G. T. Gray, and D. C. Dunand, Mater. Sci. Eng., A **391**, 408 (2005).
- <sup>30</sup>A. Rabiei and A. T. O'Neill, Mater. Sci. Eng., A **404**, 159 (2005).
- <sup>31</sup>J. Weise, V. Zanetti-Bueckmann, O. Yezerka, M. Schneider, and M. Haesche, Adv. Eng. Mater. **9**, 52 (2007).
- <sup>32</sup>A. H. Brothers and D. C. Dunand, Appl. Phys. Lett. **84**, 1108 (2004).
- <sup>33</sup>R. M. German, *Particle Packing Characteristics* (Metal Powder Industries Federation, Princeton, NJ, 1989).
- <sup>34</sup>M. F. Ashby, A. G. Evans, N. A. Fleck, L. J. Gibson, J. W. Hutchinson, and H. N. G. Wadley, *Metal Foams: A Design Guide* (Butterworth-Heinemann, Boston, 2000).
- <sup>35</sup>Q. Zheng, H. Ma, E. Ma, and J. Xu, Scr. Mater. **55**, 541 (2006).
- <sup>36</sup>M. Kiser, M. Y. He, and F. W. Zok, Acta Mater. **47**, 2685 (1999).
- <sup>37</sup>N. Gupta, E. Kishore Woldesenbet, and S. Sankaran, J. Mater. Sci. **36**, 4485 (2001).
- <sup>38</sup>Y. Yokoyama, K. Inoue, and K. Fukaura, Mater. Trans. **43**, 3199 (2002).
- <sup>39</sup>Y. Yokoyama, K. Yamano, K. Fukaura, H. Sunada, and A. Inoue, Mater. Trans. **42**, 623 (2001).
- <sup>40</sup>K. K. Chawla, *Composite Materials: Science and Engineering*, 2nd ed. (Springer, New York, 1998).